Check for updates

Janus Vitrification of Droplet via Cold Leidenfrost Phenomenon

Meng Shi, Jinbin Qiu, Shangsheng Feng, Lei Zhang, Yimin Zhao, Tian Jian Lu,* and Feng Xu*

Janus particles with asymmetric crystals show great importance in optoelectronics and photocatalysis, but their synthesis usually requires complicated procedures. Here, an unexpected Janus vitrification phenomenon is observed in a droplet caused by the Leidenfrost effect at a cryogenic temperature, which is commonly regarded as symmetric. The Leidenfrost phenomenon levitates the droplet when it comes in contact with liquid nitrogen causing different cooling conditions on the droplet's top and bottom surfaces. It induces asymmetric crystallization in the droplet, forming a Janus vitrified particle with an asymmetric crystallization borderline after cooling, as further evidenced by cryotransmission electron microscopy (cryo-TEM) experiments. Theoretical analysis and experimental study indicate that the position of the asymmetric crystallization borderline is determined by the droplet radius and density, and the observation window of asymmetric crystallization borderline is determined by the chemical concentration. The finding reveals the asymmetric crystallization phenomenon in droplet vitrification for the first time, and provides a new insight for creating Janus particles through the Leidenfrost phenomenon.

1. Introduction

Janus particles, the particles consist of two (or more) distinct sides with contrasting functionality,[1,2] have shown great promise for applications in various fields including chemistry, biotechnology, and materials science.[1–4] One of the first persons to realize the significance of such particles was the Nobel Laureate P. G. de Gennes who addressed this class of particles in his Nobel lecture in 1991,[5] where he highlighted their anisotropic physical and chemical performances. Recently, Janus particles with asymmetric crystals show great performance in the optoelectronics,[6] photocatalysis,[7,8] self-propulsion

devices,[9] and optical functional materials.[10–12] However, synthesis of these kinds of particles still requires complex fabrication devices and procedurals, such as flame breakup,[6] seeded growth,[7] e-beam evaporation,[9] microfluidic devices,[12] and so on.

In parallel, Leidenfrost phenomenon,[13] where a droplet levitates and dances on a hot plate due to its own vapor, has found widespread applications in self-propulsion, surface cooling, drag reduction and so on.[14–25] Recently, more Leidenfrost phenomena have been observed at low temperature[14,26–32] (e.g., dry ice in –78.5 °C [27] and liquid nitrogen in –196 °C [33]), which broaden its application into the low temperature arena (e.g., biology). For instance, the cold Leidenfrost phenomenon of droplet vitrification in liquid nitrogen has been widely used in cryopreservation.[33–35] When a droplet is injected into liquid nitrogen, due to the Leidenfrost phenomenon, the droplet floats on the surface of liquid nitrogen via the evaporated nitrogen vapor while it is vitrified by liquid nitrogen concurrently.[33] This droplet vitrification process has been commonly regarded as uniform and symmetric, considering that the whole droplet is surrounded by liquid nitrogen vapor at ultra-low temperature.[33–35]

However, here we observe for the first time a Janus vitrification phenomenon via Leidenfrost effect when a droplet is injected and vitrified in liquid nitrogen (Movie S1, Supporting Information), which provides an unprecedented and convenient approach to fabricate Janus particles. Due to the Leidenfrost phenomenon, the droplet is levitated on the surface of liquid

Dr. M. Shi, J. Qiu, Prof. S. Feng, Prof. F. Xu
Bioinspired Engineering and Biomechanics Center (BEBC)
MOE Key Laboratory of Biomedical Information Engineering
School of Life Science and Technology
Xi'an Jiaotong University
Xi'an 710049, P. R. China
E-mail: fengxu@mail.xjtu.edu.cn

Dr. M. Shi
Laser Thermal Laboratory
Department of Mechanical Engineering
University of California
Berkeley, Berkeley, CA 94720-1740, USA

The ORCID identification number(s) for the author(s) of this article can be found under https://doi.org/10.1002/smll.202007325.

Prof. L. Zhang, Y. Zhao
MOE Key Laboratory for Nonequilibrium Synthesis and Modulation
of Condensed Matter
School of Physics
Xi'an Jiaotong University
Xi'an 710049, P. R. China

Prof. T. J. Lu
State Key Laboratory of Mechanics and Control of Mechanical Structures
Nanjing University of Aeronautics and Astronautics
Nanjing 210016, P. R. China
E-mail: tjlu@nuaa.edu.cn

Prof. T. J. Lu
MIIT Key Laboratory of Multifunctional Lightweight Materials
and Structures (MLMS)
Nanjing University of Aeronautics and Astronautics
Nanjing 210016, P. R. China

ADVANCED
SCIENCE NEWS
www.advancedsciencenews.com

NANO · MICRO
small
www.small-journal.com
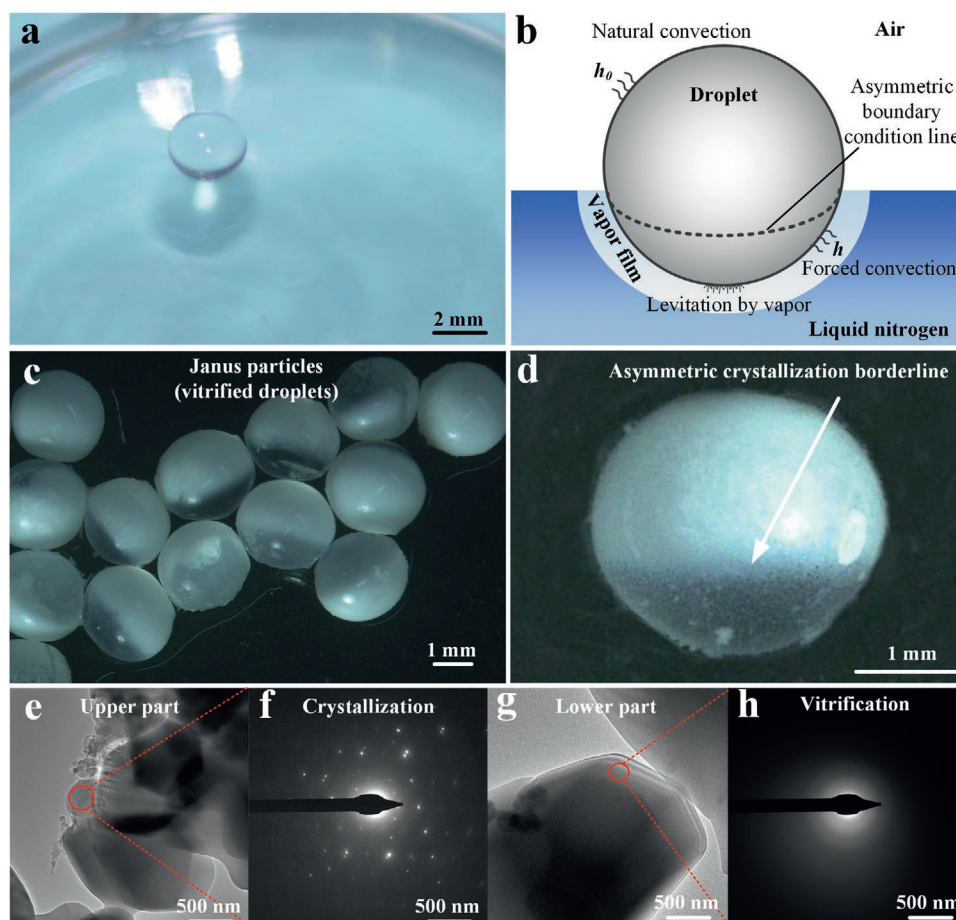
Figure 1. Janus vitrification of Leidenfrost droplet on the surface of liquid nitrogen. a) Droplet levitating on the surface of liquid nitrogen. b) Schematic of an asymmetric Leidenfrost droplet. c) Janus particles (vitrified droplets) after cooling. d) Magnified picture of a Janus particle. The white part is high crystallization (low vitrification), which is corresponding to upper part during cooling; the transparent part is low crystallization (high vitrification), which is corresponding to lower part during cooling. There is a clear asymmetric crystallization borderline separating them. e) Samples from upper part of droplet. f) Diffraction pattern of crystal structure from (e) using cryo-TEM. g) Samples from lower part of droplet. h) Diffraction pattern of vitrification structure from (g) using cryo-TEM.

nitrogen by the evaporated nitrogen vapor (**Figure 1**a). During the cooling process, this levitation behavior results in different thermal boundary conditions at the top and bottom surfaces of the droplet (Figure 1b), generating asymmetric cooling rates and corresponding asymmetric vitrification (or crystallization), finally forming a Janus particle (vitrified droplet) (Figure 1c) with a clear "Asymmetric Crystallization Borderline (termed as ACB here)" (Figure 1d). The cryo-TEM experiments evidence that the upper (Figure 1e,f) and lower part (Figure 1g,h) of particle have significantly distinguishable electron diffraction patterns. Both theoretical analysis and experimental study indicate that the position of ACB is determined by droplet radius and density, and the Janus particle can be clearly observed in the specific concentration window. Our finding not only demonstrates the asymmetric crystallization in droplet vitrification for the first time, but opens a new door for creating Janus particles through Leidenfrost phenomenon, which broadens the application of Leidenfrost phenomenon to a new arena and holds great potential in engineering, biology and materials science fields.[2–4]

2. Results

When a droplet is injected into liquid nitrogen, since the temperature of the droplet (20 °C) is much higher than that of liquid nitrogen (–196 °C), the liquid nitrogen will evaporate and form a vapor blanket around the droplet (Figure 1b). The vapor blanket provides a vapor force (F_{vd}) on the bottom of the droplet to levitate the droplet. Force balance at the interface of droplet and vapor blanket ($r = R_0$) dictates that

$$W_d = F_{vd} - F_0 \tag{1}$$

where $W_d = (4/3)\pi R_0^3 \rho_d g$ (N) is the gravity of the droplet, R_0 (m), ρ_d (kg m^{-3}), and g (m s^{-2}) being droplet radius, density and gravitational acceleration, respectively. F_0 (N) is the atmosphere pressure force and F_{vd} (N) is the vapor force underneath the droplet provided by vapor blanket, given by

$$F_0 = \int_0^{2\pi} \int_{\theta^*}^{\pi} P_0 \cos(\pi - \theta) R_0^2 \sin\theta \, d\theta \, d\varphi \tag{2}$$
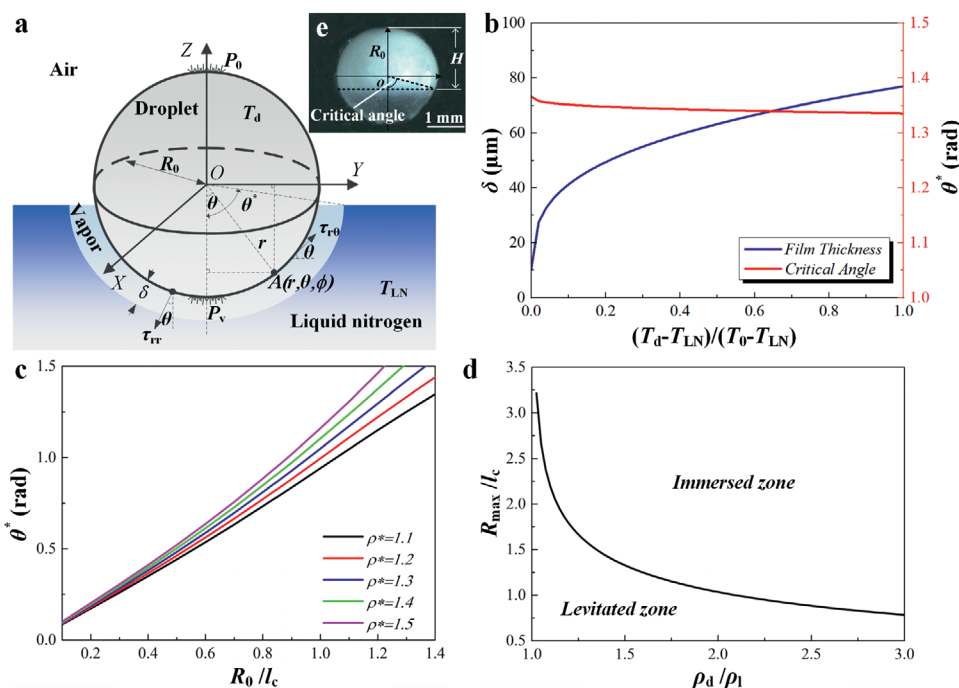
Figure 2. The critical angle and vapor film of droplet. a) Analysis sketch. b) Critical angle (θ^*) and vapor film (δ) vary with dimensionless temperature (($T_d - T_{LN})/(T_0 - T_{LN})$). c) Critical angle varies with dimensionless radius normalized by capillary length (R_0/l_c). d) Maximum dimensionless radius (R_{max}/l_c) varies with dimensionless density (ρ_d/ρ_l). e) The critical angle on the Janus particle (vitrified droplet), which is determined by measure the position of asymmetric line and calculated through $H = R_0 (1 + \cos\theta^*)$.

$$F_{vd} = \int_0^{2\pi}\int_0^{\theta^*} (P_v \cos\theta + \tau_{r\theta}\sin\theta - \tau_{rr}\cos\theta)R_0^2 \sin\theta d\theta d\varphi \quad (3)$$

where r, θ, φ are the spherical coordinates. θ^* (rad) is the critical angle of the levitated droplet, decided by the height of the droplet immersed in liquid nitrogen (**Figure 2**a,e). P_0 (Pa) is the atmosphere pressure. P_v (Pa) is the pressure in the vapor film. $\tau_{r\theta} = \mu\left(r\frac{\partial}{\partial r}\left(\frac{v_\theta}{r}\right)\right)\Big|_{r=R_0}$ (Pa) and $\tau_{rr} = 2\mu\left(\frac{\partial v_r}{\partial r}\right)\Big|_{r=R_0} \approx 0$ (Pa) are the tangential and radial components of the shear stress of vapor,[36] respectively. Besides, μ (Pa s) is the dynamic viscosity of nitrogen vapor, while v_θ (m s^{-1}) and v_r (m s^{-1}) are the tangential and radial velocity components of nitrogen vapor, respectively.

At the interface of vapor blanket and liquid nitrogen, the vapor pressure pushes down the surface of liquid nitrogen, inducing deformation of the surface. Corresponding, force balance of the vapor force, the hydraulic pressure force, and the surface tension of liquid nitrogen can be given as

$$F_{vl} = F_b + F_\sigma \quad (4)$$

where F_{vl} (N) is the vapor force at the interface between vapor and liquid nitrogen, F_b is the hydraulic pressure force (N) and F_σ (N) is the surface tension at the vapor-liquid interface. These forces can be calculated as

$$F_{vl} = \int_0^{2\pi}\int_0^{\theta^*} P_v \cos\theta (R_0 + \delta)^2 \sin\theta d\theta d\varphi \quad (5)$$

$$F_b = \int_0^{2\pi}\int_0^{\theta^*} P_l \cos\theta (R_0 + \delta)^2 \sin\theta d\theta d\varphi \quad (6)$$

$$F_\sigma = \int_0^{2\pi}\int_0^{\theta^*} \left(\frac{2\sigma}{R_0 + \delta}\right)\cos\theta (R_0 + \delta)^2 \sin\theta d\theta d\varphi \quad (7)$$

where $P_l = P_0 + (R_0 + \delta)(\cos\theta - \cos\theta^*)(\rho_l - \rho_v)g$ (Pa) is the hydraulic pressure of liquid nitrogen at vapor-liquid interface. δ (m) is the thickness of vapor blanket. ρ_l and ρ_v (kg m^{-3}) are separately the density of liquid nitrogen and nitrogen vapor,[37] and σ (N m^{-1}) is the surface tension coefficient of liquid nitrogen.[38]

Compared to the droplet radius (in this work, ≈1.3 mm), the vapor film is usually much thinner (≈0.1 mm). Correspondingly, with the representative velocity of vapor film ≈1 m s^{-1} and the kinetic viscosity of liquid nitrogen 1.38×10^{-5} m^2 s^{-1}, the Reynolds number is ≈7.2. Thus, the vapor flow in the vapor blanket is a typical thin film flow in small Reynolds number regime, and it can be regarded as a laminar flow so that the lubrication approximation can be applied. The vapor flow obeys the reduced continuity equation and momentum equations[39]

$$0 = \frac{1}{r^2}\frac{\partial(r^2 v_r)}{\partial r} + \frac{1}{r\sin\theta}\frac{\partial(v_\theta \sin\theta)}{\partial\theta} \quad (8)$$

$$0 = -\frac{\partial P_v}{\partial r} \quad (9)$$

$$0 = -\frac{1}{r}\frac{\partial P_v}{\partial\theta} + \mu\frac{\partial^2 v_\theta}{\partial r^2} \quad (10)$$

With the upper and bottom boundaries satisfying nonslip boundary conditions, the velocity of vapor meets $v_\theta = 0$ at $r = R_0$ and $r = R_0 + \delta$. Through Equations (8–10), the variation of vapor velocity and pressure profile with vapor flow rate $Q(\theta)$ ($m^3 s^{-1}$) can be obtained.

As the energy of liquid nitrogen evaporation is derived from the heat transfer between the liquid nitrogen and the droplet and the heat brought by nitrogen vapor could be ignored compared to the latent heat of evaporation (198 kJ kg^{-1}), the evaporation rate of liquid nitrogen can be given as

$$M(\theta)L = \rho_v Q(\theta)L = hA_1(T_d - T_{LN}) \tag{11}$$

where $M(\theta)$ (kg s^{-1}) is the evaporation mass rate of liquid nitrogen, and L (J kg^{-1}) is the latent heat of evaporation of liquid nitrogen. T_d (K) and T_{LN} (K) are the temperatures of the droplet and liquid nitrogen, respectively.[40] A_1 (m^2) is the surface area of the bottom part of the droplet. h (W m^{-2} K^{-1})) is the heat transfer coefficient between the droplet and liquid nitrogen.[41] Through Equations (8–11), the vapor velocity and pressure profile can be written as

$$v_\theta(r,\theta) = \frac{6R_0 h(T_d - T_{LN})}{\delta^3 \rho_v L}\left(\frac{1-\cos\theta}{\sin\theta}\right)(R_0 + \delta - r)(r - R_0) \tag{12}$$

$$P_v(\theta) = P_0 + \frac{12\mu h R_0^2 (T_d - T_{LN})}{\delta^3 \rho_v L}\ln\left(\frac{1+\cos\theta}{1+\cos\theta^*}\right) \tag{13}$$

Introducing Equations (12) and (13) into Equations (1–7), we can establish the relationship between the critical angle θ^*, the thickness of vapor blanket δ, and the dimensionless temperature of droplet $(T_d - T_{LN})/(T_0 - T_{LN})$. The additional theoretical analysis can be found in the Supporting Information. The tangential components of shear stress induced by vapor at the bottom of the droplet are

$$\tau_{r\theta}\big|_{r=R_0} = \frac{6\mu_v R_0 h(T_d - T_{LN})}{\delta^2 \rho_v L}\tan\frac{\theta}{2} \tag{14}$$

The net vapor torque Γ(N m) acting on the bottom of droplet is

$$\Gamma = R_0 \int_0^{2\pi}\int_0^{\theta^*} \tau_{r\theta}R_0^2 \sin\theta d\theta d\varphi + R_0 \int_0^{2\pi}\int_0^{-\theta^*} \tau_{r\theta}R_0^2 \sin\theta d\theta d\varphi = 0 \tag{15}$$

That is, due to the symmetry of droplet, the net rotation torque acting on the droplet can be taken as zero. Consequently, when the droplet levitates on the surface of liquid nitrogen, it hardly rolls. Moreover, small fluctuations on the surface of liquid nitrogen could induce asymmetricity in vapor film, which will result in a propulsion movement of droplet on the surface of liquid nitrogen (Movie S1, Supporting Information). However, the droplet will only glide on the surface without rotation, due to the balance of propelling and friction forces in the vapor film.[42]

During cooling, the temperature of the droplet (T_d) and the crystallization process simultaneously vary with cooling time, which are coupled and governed by[43]

$$\rho_d c_{p,d}\frac{\partial T_d}{\partial t} = k_d \nabla^2 T_d + \rho_d L_d \frac{d\chi}{dt} \tag{16}$$

$$\frac{d\chi}{dt} = k_a \chi^{\frac{2}{3}}(1-\chi)(T_m - T_d)e^{-\frac{Q}{RT_d}} \tag{17}$$

where k_d (W m^{-1} K^{-1}), $c_{p,d}$ (J kg^{-1} K^{-1}), and L_d (J kg^{-1}) are the thermal conductivity, the specific heat and the latent heat of the droplet,[44] respectively, t (s) is the time, χ represents the fraction of crystallization ($0 < \chi < 1$), T_m is the melting temperature, Q (J mol^{-1}) is the activation energy, R (J mol^{-1} K^{-1}) is the gas constant, and k_a (K s^{-1}) is the characteristic coefficient of crystallization.

Due to the Leidenfrost phenomenon, the immersed (under the ACB) and nonimmersed (above the ACB) parts of the droplet have different boundary conditions (Figure 1b). Since the immersed part is bathed in the liquid nitrogen and its vapor blanket (temperature: ≈77 K in the liquid nitrogen), it is regarded as the forced convection boundary and the heat transfer coefficient h is obtained from Equation S11 in the Supporting Information. As the nonimmersed part is exposed in the air and nitrogen vapor (temperature: ≈ 185 K at ≈1.3 mm above the surface of liquid nitrogen, as experimentally measured by thermocouple), it is regarded as the natural convection boundary and its heat transfer coefficient h_0 is set as 10 W m^{-2} K^{-1}). Such asymmetric boundary conditions lead to asymmetric cooling rate in the droplet, which induces asymmetric crystallization and finally forms a Janus particle (vitrified droplet). As the distance of ACB from the top of Janus particle (H (m)) is given by $H = R_0 (1 + \cos\theta^*)$ (Figure 2a,e) and the immersed critical angle (θ^*) is determined by droplet density and radius, the boundary conditions are different in different droplets due to changes in the ACB position.

As a representative, we chose the 10 µL of 35% 1,2-propanediol (The mixture of 1,2-propanediol (CAS number: 57-55-6, purity: >99.0%, Tianjin Fuyu Fine Chemical Co. Ltd.) and deionized water for experimental and theoretical investigation of the asymmetric vitrification phenomenon in this study, which is a common cryoprotective agent (CPA) used in cryopreservation.[45] It has a critical cooling rate of ≈294 K min^{-1} when crystallization fraction is less than 0.5%.[46] During experiments, a pipette was used to accurately generate the droplets and its tip was positioned to the liquid nitrogen surface as close as possible. Then the droplets were gently ejected to the calmed liquid nitrogen surface, and then levitated and cooled by the generated nitrogen vapor underneath (Movie S1, Supporting Information). After droplets immersed into liquid nitrogen, they became Janus particles which were utilized for imaging measurements and cryo-TEM experiments. During all the processes, the particles were kept in the liquid nitrogen environment to prevent any rewarming. The detailed procedures are described in the Experimental Section.

The cryo-TEM experiments indicate that, there are significantly distinguishing electron diffraction patterns in the upper and lower part of the vitrified Janus particle (Figure 1e–h). The materials show a crystallization pattern with clear and regular crystal lattices in the upper (white) region of particle (Figure 1e,f), but a vitrification pattern whose profile is typically the same as classical amorphous solids in the lower (transparent)
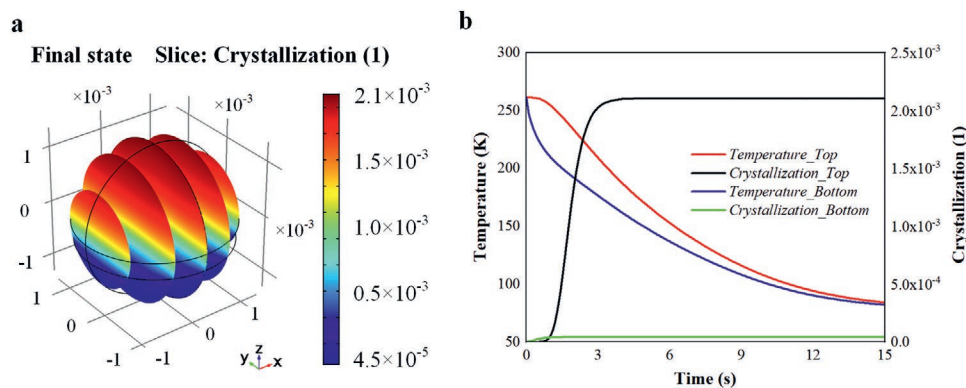
Figure 3. Crystallization calculations of Janus vitrification of droplet. a) Slices view of Crystallization distribution in Janus particle. The upper part has higher crystallization (red) and the lower part has lower crystallization (blue). b) Variation of temperature and crystallization at the top and bottom of droplet. Temperature variation of the lower part of the droplet (Blue line) is much higher than the upper part (red line), which induces the significant difference of crystallization in the lower part of the droplet (green line) and the upper part (black line).

region (Figure 1g,h). These results provide a solid evidence for the formation of Janus vitrification/crystallization in one droplet due to Leidenfrost phenomenon in liquid nitrogen.

To calculate the critical angle ($\theta*$) of this droplet, we first solved Equations (1–13) in MATLAB software using the parameters listed in Table S1 in the Supporting Information (Table S1, Supporting Information). To verify the validity of employing the approximation of small Reynolds number flow and lubrication analysis in this work, we calculated the film thickness and critical angle at initial time and then computed the velocity of vapor flow and the corresponding Reynolds number in vapor film. The results indicated that, the vapor film ($\approx$77 μm) is sufficient thin compared to the droplet radius ($\approx$1.3 mm) and the tangential vapor velocity is calculated as $\approx$1.8 m s^{-1}, which results in the Reynolds number in vapor film of $\approx$10. That is, the aforementioned approximation of small Reynolds number flow and lubrication analysis in this work can be well accepted.

Further, through calculations, we obtained the relationship between the critical angle θ^*, the film thickness of vapor blanket δ, and the dimensionless temperature of the droplet $(T_d - T_{LN})/(T_0 - T_{LN})$ (Figure 2b). The film thickness decreases with reduction of droplet temperature (T_d). Interestingly, the critical angle rarely changes (from 1.32 to 1.37 rad) between the melting temperature ($T_m = 255$ K[47]) and the glass transition temperature ($T_g = 153$ K[48]) of the droplet (Figure 2b), which agrees well with the experimental results (measured critical angle: $\approx$ 1.32 rad). This result indicates that the boundary condition of droplet rarely changes between the melting temperature and the glass transition temperature, which is the temperature regime for crystallization formation. As a result, the cooling conditions of droplet remain stable during the entire cooling process so that stable asymmetric crystallization can be formed in the droplet. At the same time, we explored the variation of critical angle with droplet radius normalized by the capillary length of liquid nitrogen (R_0/l_c, $l_c = (\sigma/(\rho_l g))^{1/2}$). We found that, in the current vitrification system, the critical angle is determined by the radius and density of droplet, and it increases with increasing radius and density (Figure 2c). Besides, since the levitation of droplet is controlled by the buoyancy force (and surface tension) of liquid nitrogen which has a maximum

value, there exists a maximum dimensionless droplet radius (R_{max}/l_c) which is dependent upon the dimensionless density (ρ_d/ρ_l) (Figure 2d).

Then, we utilized the above calculated critical angle to set the cooling boundary conditions of the droplet, and calculated crystallization distribution in the droplet by solving Equations (16) and (17) in the COMSOL software (**Figure 3**). The results indicate that there is a significant difference of crystallization formed in the upper and lower parts of the droplet, as reflected by the clear layers with distinguishable crystallization in the Janus particle (Figure 3a). This is attributed to the dramatically different cooling rates (during initial 1 s: top: $\approx$ 420 K min^{-1}; bottom: $\approx$ 3120 K min^{-1}) in the droplet, as caused by the Leidenfrost phenomenon (Figure 3b). Thus, higher crystallization occurred at the top of droplet while lower crystallization occurred at the bottom (Figure 3a). Since crystallization with sharp contrast was created in one droplet, the Janus particle with asymmetric crystallization was observed clearly after cooling.

To explore the effect of droplet properties (e.g., radius, density) on the critical angle (ACB position), we performed droplet vitrification experiments by ejecting droplets with different radii and densities into liquid nitrogen. The radius of droplets was varied by their volume (V_d (μL)), and the density of droplets was tuned by adding different mass fractions of glass microbeads (diameter: 75 ± 25 μm, density: 2500 kg/m^3) into the liquids. After cooling, the images of Janus particles were taken in the liquid nitrogen to avoid the recrystallization process. Then, we measured the distance of ACB from the top of particle (H) (Figure 2e) through images processing and calculated the corresponding experimental critical angle (θ^*) (**Figures 4** and **5**).

Through experiments, we observed that the distance of ACB from the top of Janus particle decreases significantly while the corresponding critical angle increases with increasing droplet volume (i.e., droplet radius) (Figure S1, Supporting Information). To explain such observation, we calculated the variation of critical angle (θ^*) with droplet volume (Figure 4a, blue curve) and compared with the experimental results (Figure 4a, black points). The results indicate that, the critical angle increases with increasing droplet radius, which agrees well with the experimental results. The reason is that, when the droplet
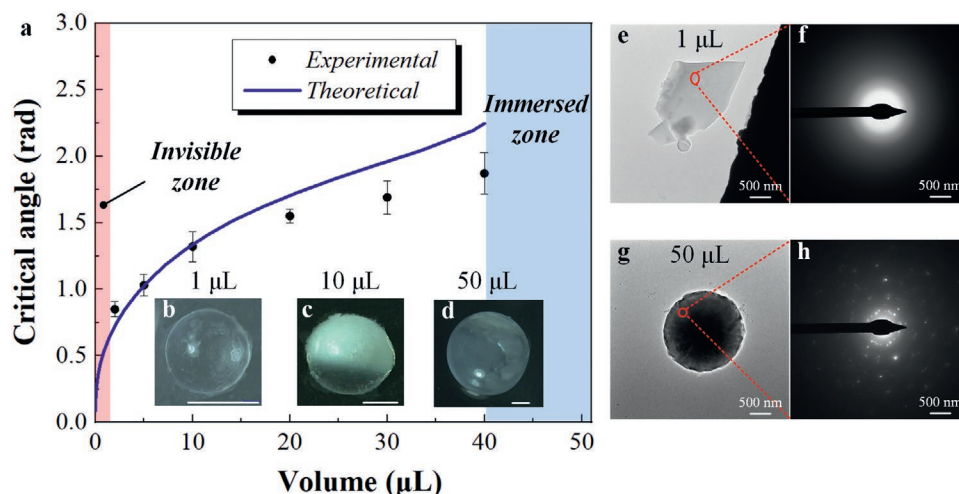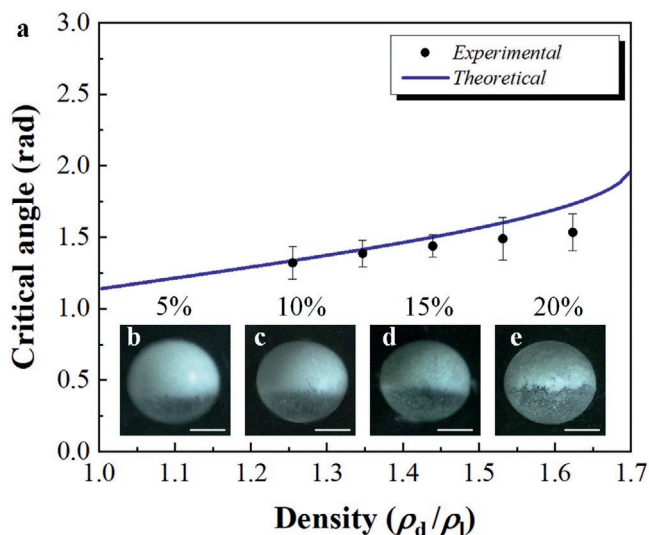
Figure 4. The effect of droplet volume on the asymmetric crystallization. a) Critical angle varies with the volume of 35% 1,2-propanediol droplet (Blue curve: theoretical results; Black points: experimental results). b) If the droplet is smaller than 2 µL, (e.g., 1 µL), the asymmetric crystallization borderline disappears (Invisible zone: red region) due to low crystallization and similar cooling boundaries. c) From 2 µL to 40 µL, the asymmetric crystallization borderline can be clearly seen on the droplet. d) If the droplet volume is larger than 40 µL (e.g., 50 µL), the asymmetric crystallization borderline disappears due to immersion (Immersed zone: blue region). Scale bar: 1 mm. e) Samples from 1 µL droplet. f) Diffraction pattern of vitrification structure from (e) using cryo-TEM. g) Samples from 50 µL droplet. h) Diffraction pattern of crystal structure from (g) using cryo-TEM.

radius increases, the gravity of droplet increases, causing the vapor pressure underneath the droplet to grow, thus providing increasing levitation force. Compared to a small droplet, the increase of vapor force under a large droplet will induce a larger deformation of the liquid nitrogen interface. Consequently, the larger droplet is immersed deeper and hence the critical angle of Janus particle is increased.

However, we did not observe clear ACB on the particles when droplet volume decreases to <2 µL (Figure 4a, Invisible zone) or increases to >40 µL (Figure 4a, Immersed zone). There are two possible reasons for small droplets: 1) A

Figure 5. The effect of droplet density on the asymmetric crystallization. a) Critical angle varies with the droplet density as tuned by adding glass microbeads. Representative pictures of 10 µL 35% 1,2-propanediol droplets mixed with different mass fractions of glass microbeads after cooling: b) 5%; c) 10%; d) 15%; e) 20%. Scale bar: 1 mm.

smaller droplet is easier to be vitrified. If the droplet is sufficiently small (<2 µL), even there is difference of crystallization within one droplet, the fraction of crystallization is too small to be observed and the ACB on the particle cannot be clearly observed; 2) A vapor layer always exists all over the surface of liquid nitrogen, which becomes colder as the liquid nitrogen is approached. Thus, although a small droplet levitates on the surface of liquid nitrogen, its location is close to the surface of liquid nitrogen where the cold vapor exists. Thus, both the top and bottom of the small droplet are wreathed by the similarly cold vapor, and hence their cooling boundary conditions are comparable. Therefore, the difference in crystallization is too small to be distinguished and the ACB on the particle is hard to be observed (Figure 4b). When the droplet becomes larger, the asymmetricity of cooling boundary conditions and crystallization will increase, and thus the ACB can be observed (Figure 4c). However, if a droplet is sufficiently large (>40 µL), it could totally be immersed in the liquid nitrogen ($\theta^* = 180°$) during cooling. As a result, the cooling boundary of the entire droplet will be the same and the droplet has a uniform crystallization, which induces the ACB disappeared (Figure 4d). For illustration, we calculated the crystallization in 1 µL and 50 µL droplets after cooling, and the results indeed indicate that there is no clear ACB on these particles (Figure S2a,b, Supporting Information). We also performed the cryo-TEM experiments on the droplets with the volume of 1 µL and 50 µL after cooling. Since there is no clear ACB on these cooled droplets, the samples from multiple positions of cooled droplets were taken to test in the cryo-TEM (Figure S2c,d, Supporting Information), and representative pictures of electron diffraction patterns are shown in Figure 4e–h. The results show that there are mostly vitrification patterns in the 1 µL cooled droplet (Figure 4f; Figure S2c, Supporting Information). In comparison, the 50 µL cooled droplet has more crystallization patterns than vitrification patterns (Figure 4h; Figure S2d, Supporting Information).

**ADVANCED
SCIENCE NEWS**
www.advancedsciencenews.com

**NANO · MICRO
small**
www.small-journal.com

These findings can be a molecular-level reference for choosing proper sizes of droplets using in droplet vitrification.

To investigate the effect of droplet density on the critical angle, we added different mass fractions (5%, 10%, 15%, 20%) of glass microbeads (diameter: 75 ± 25 μm, density: 2500 kg m^{-3}) into the 35% 1,2-propanediol solution. Since the high density and chemical stability of glass microbeads, we could obtain droplets with different densities without bringing any chemical issues. After cooling experiments, we observed that the distance of ACB from the top of Janus particle (cooled droplet) decreases gradually while the corresponding critical angle increases with increasing droplet density (Figure 5). To explain the observation, we calculated the variation of critical angle (θ^*) with droplet density (Figure 5a, blue curve) and compared it with the experimental results (Figure 5a, black points), which were obtained from the pictures of droplets after cooling (Figure 5b–e). The results indicate that the critical angle increases with increasing droplet density, which results in an increase of the droplet gravity, causing a larger deformation of the liquid nitrogen interface. Consequently, a denser droplet

is immersed deeper, and hence the critical angle of the Janus particle is increased.

To investigate the effect of chemical concentration on Janus vitrification, we tuned the chemical concentration of 1,2-propanediol in droplets from 0% to 100% (Figure S3, Supporting Information) and measured the critical angle (**Figure 6**). However, we observed that the ACB only can be clearly seen when the chemical concentration in droplets falls within the range from 33.75% (V/V) to 38.75% (V/V) (Figure 6c). Correspondingly, the critical angle slightly increases with the increasing droplet concentration in this region (Figure 6a), but the critical angle does not vary significantly as the droplet density changes in a narrow range. Interestingly, if the chemical concentration in droplet is < 33.75% or > 38.75%, the ACB will disappear (Figure 6a, Invisible zone). The reason is that, a low concentration of chemical droplet has a high critical cooling rate for its vitrification,[49] if the chemical concentration is less than 33.75%, the whole droplet will form a high crystallization due to the high critical cooling rate. Even the asymmetric crystallization does still exist, the high crystallization makes the transparency of entire droplet
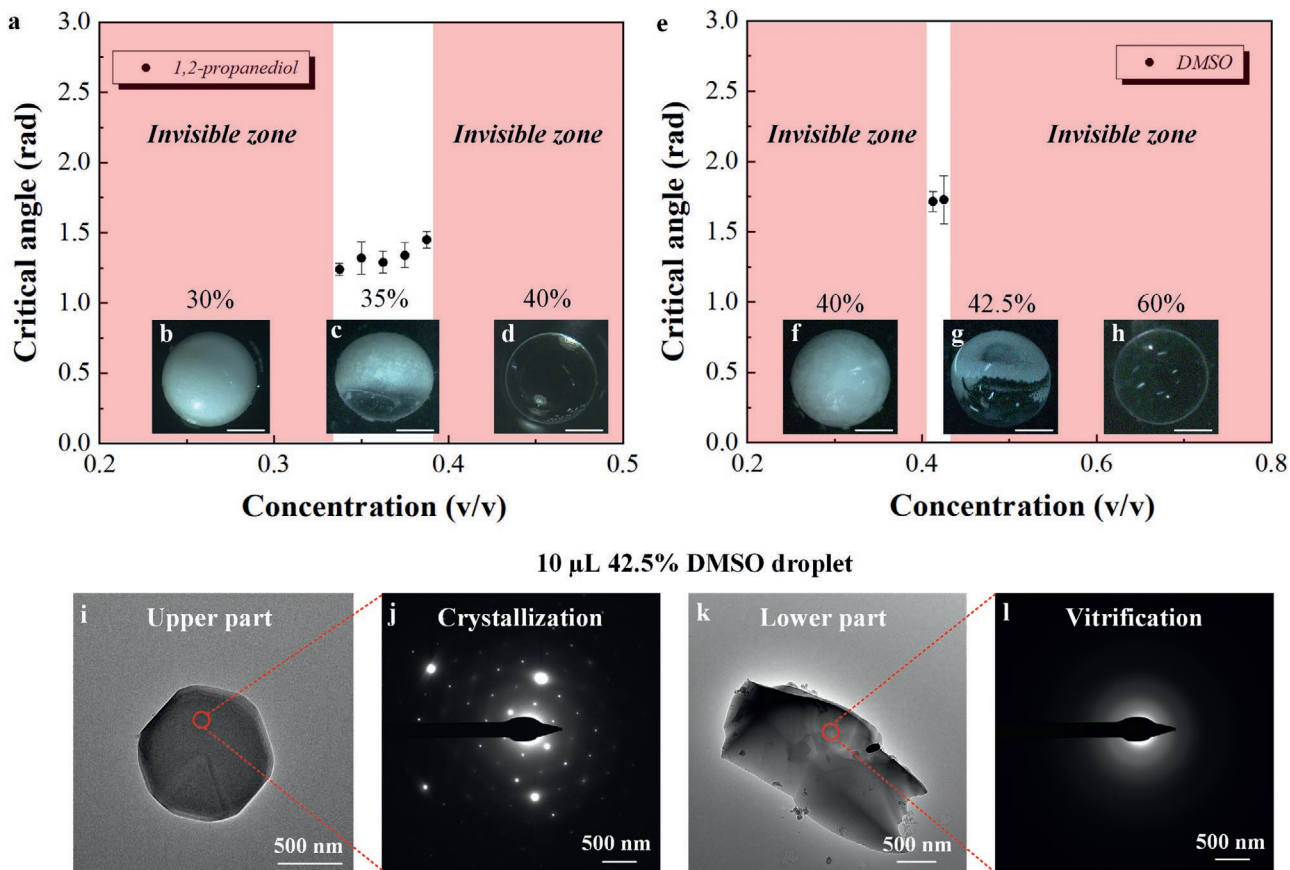
Figure 6. The effect of chemical concentration in droplet on the asymmetric crystallization. a) Critical angle varies with the chemical concentration of 1,2-propanediol droplet. Representative pictures of droplets with different concentrations after cooling: b) 30%, in the ACB invisible zone (red region) when droplet concentration is lower than 33.75%; c) 35%, in the ACB concentration window of 1,2-propanediol, ranging from 33.75% to 38.75%; d) 40%, in the ACB invisible zone when droplet concentration is higher than 38.75%. e) Critical angle varies with the chemical concentration of the DMSO droplet. Representative pictures of droplets with different concentrations after cooling: f) 40%, in the ACB invisible zone (red region) when droplet concentration is lower than 41.25%; g) 42.5%, in the ACB concentration window of DMSO, ranging from 41.25% to 42.5%; h) 60%, in the ACB invisible zone when droplet concentration is beyond 42.5%. Scale bar: 1 mm. Cryo-TEM experiments on a 10 μL 42.5% DMSO droplet after cooling: i) Samples from upper part of droplet; j) Diffraction pattern of crystal structure from (i); k) Samples from lower part of droplet; l) Diffraction pattern of vitrification structure from (k).

significantly decreased, and hence ACB on the Janus particle cannot be observed (Figure 6b). Similarly, if the chemical concentration exceeds 38.75%, the whole droplet will form a low crystallization (high transparency) due to the low critical cooling rate so that it is also difficult to observe ACB on the Janus particle (Figure 6d). As an example, we calculated the crystallization of droplets with 30% and 40% 1,2-propanediol after cooling, and the results confirmed that there is no clear ACB on the particles (Figure S4, Supporting Information). Therefore, the ACB observation window of 1,2-propanediol is that the chemical concentration ranges from 33.75% (V/V) to 38.75% (V/V).

To explore the Janus vitrification phenomenon on other liquids, we performed droplet vitrification on the 10 µL droplets of the mixture of DMSO and deionized water. We tuned the chemical concentration of DMSO in droplets from 5% to 80% (Figure S5, Supporting Information) and measured the critical angle after cooling (Figure 6e). Interestingly, we found that the ACB concentration window of DMSO ranges from 41.25% to 42.5%. (Figure 6e). As examples, the ACB can be clearly seen on the cooled droplets with a DMSO concentration of 42.5%, but it cannot be observed on the droplets with DMSO concentrations of 40% and 60% (Figure 6f–h). Representatively, we took samples from the upper and lower regions of a cooled droplet with a concentration of 42.5% separately to test their electron diffraction patterns in the cryo-TEM. The materials from the upper (white) region of the cooled droplet show a crystallization pattern with clear and regular crystal lattices (Figure 6i,j), while the materials from the lower (transparent) region show a vitrification pattern (Figure 6k,l). In other words, the Janus vitrification/crystallization was also formed in the DMSO droplet due to the Leidenfrost phenomenon in liquid nitrogen. In the invisible zones (red regions in Figure 6e) where the droplet concentration below 41.25% and beyond 42.5%, we believe that they result from the high crystallization and high vitrification in the entire droplets, respectively, which is similar to 1,2-propanediol.

3. Discussion

The above finding of this new phenomenon not only reveals that the direct cooling of a droplet in the liquid nitrogen is an asymmetric process, more importantly, it opens a new door to create Janus particles conveniently by utilizing the Leidenfrost phenomenon. Although we utilized 1,2-propanediol and DMSO droplets on liquid nitrogen in this work for initial exploration, such Janus vitrification phenomenon is not limited to them and it could be found and utilized in other kinds of liquid droplets (e.g., melted metal/alloy, glycerol) that can levitate on the surface of other cool liquids (e.g., water, liquid oxygen). For instance, if we eject a hot melted metal droplet into room temperature water, with optimized parameters, the droplet will be levitated on the surface of the water by the Leidenfrost phenomenon and be cooled down by the water and surrounding gases. At the final state, the droplet will have a different crystallization between its top and bottom (not only different fractions but also different crystal patterns), thus forming a Janus metal particle which has asymmetric properties. These kinds of Janus metal/alloy particles have already been employed in the optoelectronics,[6] photocatalysis[7] and optical manipulation.[10]

For perspective, with this approach, more novel multi-functional Janus particles could be created through tuning the droplet materials and cooling agents.

However, a large volume droplet (e.g., >50 µL for 1,2-propanediol used in the current study) may not be suitable for Janus vitrification, since it will easily drop into the liquid pool after ejection (i.e., no levitation). A recent study provided a droplet density dependent critical radius for identifying if the droplet can levitate on the liquid nitrogen,[29] which also could help to choose a proper droplet for levitation. Besides, since a low viscosity droplet (e.g., water) is hard to be vitrified and high thermal stresses will be induced by crystal formation in the droplet, the low viscosity droplet will be more likely to crack upon cooling in liquid nitrogen. Consequently, the application of Janus vitrification is also affected by the viscosity of droplet. What's more, gas may be dissolved in the droplet which may have a slight effect on the Janus vitrification, since the gas in the droplet will come out from the liquid and get trapped when the droplet gets cold and freezes. Thus, a degassing procedure before cooling might be necessary if the liquids contain high fractions of gas.

Additionally, we assumed that the thermal properties of the droplet remain unchanged since the thermal properties of 1,2-propanediol do not vary significantly in the temperature range studied.[50] In addition, we assumed that the vapor film under the droplet is uniform since it is very thin compared to droplet radius, typically <1% of droplet radius, which cannot induce large difference in vapor pressure since the vapor pressure is dominated by droplet gravity. In the future, we will reexamine these assumptions to optimize our theoretical model and the different liquids with different thermal properties will be investigated as well.

4. Conclusion

In conclusion, we observed for the first time the Janus vitrification phenomenon in a droplet as induced by Leidenfrost phenomenon when it is injected into liquid nitrogen. Through theoretical and experimental analyses, we found that the position of ACB on the Janus particle is affected by the radius and density of the droplet. That is, the critical angle increases with increasing droplet radius and density due to increasing gravity. Moreover, the observation window of ACB is determined by the chemical concentration of the droplets. As a representative, for a commonly used cryoprotective agent in cryopreservation (i.e., 1,2-propanediol), the Janus particle can be clearly observed in a specific chemical concentration region (33.75–38.75% (V/V)). This new phenomenon may open a new door to create novel Janus particles via Leidenfrost phenomenon, which holds great potential in materials science, chemistry, biology and other fields.

5. Experimental Section

Droplet Experiments: The liquid nitrogen was first poured into 3 ml culture dishes and let it boil until the surface become calm. The mixture of 1,2-propanediol (CAS number: 57-55-6, purity: >99.0%, Tianjin Fuyu Fine Chemical Co. Ltd.) and deionized water was used as the representative droplets explored in this work. The mixture of DMSO (CAS number: 67-68-5, purity: >99.7%, Tianjin Fuyu Fine Chemical Co.

**ADVANCED
SCIENCE NEWS**

www.advancedsciencenews.com

**NANO · MICRO
small**

www.small-journal.com

Ltd.) and deionized water also was used as the droplets to explore the chemical concentration effect. The density of droplets was tuned by adding the different mass fractions of glass microbeads (diameter: $75\pm25~\mu m$, density: $2500~kg~m^{-3}$) into liquids, and the different chemical concentrations of liquids were prepared by a graduated cylinder. All the droplets were accurately generated by a pipette, and then gently injected on the surface of liquid nitrogen. The pipette tip was positioned to the liquid nitrogen surface as close as possible when injecting. After cooling, the images of Janus particles were taken in the liquid nitrogen to avoid the recrystallization process. The images and videos were taken by an optical microscopy of ultra-depth field (KEYENCE, VHX-600E), and a digital camera (NIKON, D90). The data of the asymmetric crystallization borderline (i.e., the distance of ACB from the top of droplet (H)) were systematically measured from images processing and the corresponding experimental critical angles (θ^*) were calculated by $H = R_0 (1 + \cos\theta^*)$. The temperatures in the liquid nitrogen and liquid nitrogen vapor were measured by the T type thermocouple.

Cryo-TEM Experiments: A frozen Janus particle was kept in a dish filled with liquid nitrogen, while the white part (high crystallization side) of the droplet was placed towards the left. Then the droplet was fixed by a tweezer precooled by liquid nitrogen and then smashed into powders by a precooled Polytetrafluoroethylene (PTFE) hammer in liquid nitrogen. Therefore, the powders of the white part were located on the left side, while the powders of the transparent part were on the right side. While immersed in liquid nitrogen, the powders from the left and right sides were transported separately onto the Gatan 626 cryo-TEM holders, and isolated from the environment by a tightly closed shutter. During insertion into the TEM column, the temperature of the sample was kept below −170 °C. Cryo-TEM micrographs were acquired at −180 °C on a FEI CETA 4k × 4k CMOS camera by a FEI F200C transmission electron microscope (TEM) operating at 200-kV and low-electron-dose conditions. Selected-area electron diffraction (SAED) images were taken with a ≈350 nm diameter selected-area (SA) aperture. The exposure time was tuned between 0.5 and 2 s, and the binning 2 was adopted for acquiring the images.

Calculations: To calculate the critical angle (θ^*) of this droplet, we first solved Equations. (1) to (15) in MATLAB (2016b) software using the parameters listed in Table S1 in the Supporting Information (Table S1, Supporting Information). Then we utilized the critical angle to set the cooling boundary conditions of the droplet, and calculated crystallization distribution in the droplet by solving Equations (16) and (17) in COMSOL software (COMSOL 5.0). The thickness and velocity of vapor film, the effects of droplet volume and density were calculated by MATLAB, and the crystallization and temperature of Janus particles were calculated in CMOSOL.

Supporting Information

Supporting Information is available from the Wiley Online Library or from the author.

Acknowledgements

Conflict of Interest

The authors declare no conflict of interest.

Data Availability Statement

Data sharing is not applicable to this article as no additional data were created or analyzed in this study.

Keywords

[1] A. Walther, A. H. Muller, *Chem. Rev.* **2013**, *113*, 5194.
[2] L. C. Bradley, K. J. Stebe, D. Lee, *J. Am. Chem. Soc.* **2016**, *138*, 11437.
[3] Z. Rozynek, A. Mikkelsen, P. Dommersnes, J. O. Fossum, *Nat. Commun.* **2014**, *5*, 3945.
[4] T. Nisisako, *Curr. Opin. Colloid Interface Sci.* **2016**, *25*, 1.
[5] P. G. Degennes, *Science* **1992**, *256*, 495.
[6] A. Gumennik, E. C. Levy, B. Grena, C. Hou, M. Rein, A. F. Abouraddy, J. D. Joannopoulos, Y. Fink, *Proc. Natl. Acad. Sci. USA* **2017**, *114*, 7240.
[7] Y. Ben-Shahar, F. Scotognella, I. Kriegel, L. Moretti, G. Cerullo, E. Rabani, U. Banin, *Nat. Commun.* **2016**, *7*, 10413.
[8] A. Chauhan, M. Rastogi, P. Scheier, C. Bowen, R. V. Kumar, R. Vaish, *Appl. Phys. Rev.* **2018**, *5*, 041111.
[9] B. Jang, A. Hong, H. E. Kang, C. Alcantara, S. Charreyron, F. Mushtaq, E. Pellicer, R. Büchel, J. Sort, S. S. Lee, *ACS Nano* **2017**, *11*, 6146.
[10] O. Ilic, I. Kaminer, B. Zhen, O. D. Miller, H. Buljan, M. Soljačić, *Sci. Adv.* **2017**, *3*, 1602738.
[11] L. Wang, Y. Rho, W. Shou, S. Hong, K. Kato, M. Eliceiri, M. Shi, C. P. Grigoropoulos, H. Pan, C. Carraro, *ACS Nano* **2018**, *12*, 2231.
[12] Y. Hu, J. Wang, C. Li, Q. Wang, H. Wang, J. Zhu, Y. Yang, *Langmuir* **2013**, *29*, 15529.
[13] B. Gottfried, C. Lee, K. Bell, *Int. J. Heat Mass Transfer* **1966**, *9*, 1167.
[14] T. M. Schutzius, S. Jung, T. Maitra, G. Graeber, M. Köhme, D. Poulikakos, *Nature* **2015**, *527*, 82.
[15] J. Li, Y. Hou, Y. Liu, C. Hao, M. Li, M. K. Chaudhury, S. Yao, Z. Wang, *Nat. Phys.* **2016**, *12*, 606.
[16] G. Lagubeau, M. L. e. Merrer, C. Clanet, D. Quéré, *Nat. Phys.* **2011**, *7*, 395.
[17] A. Würger, *Phys. Rev. Lett.* **2011**, *107*, 164502.
[18] H. Linke, B. J. Alemán, L. D. Melling, M. J. Taormina, M. J. Francis, C. C. Dow-Hygelund, V. Narayanan, R. P. Taylor, A. Stout, *Phys. Rev. Lett.* **2006**, *96*, 154502.
[19] S. R. Waitukaitis, A. Zuiderwijk, A. Souslov, C. Coulais, M. van Hecke, *Nat. Phys.* **2017**, *13*, 1095.
[20] D. Quéré, *Annu. Rev. Fluid Mech.* **2013**, *45*, 197.
[21] T. R. Cousins, R. E. Goldstein, J. W. Jaworski, A. I. Pesci, *J. Fluid Mech.* **2012**, *696*, 215.
[22] I. U. Vakarelski, N. A. Patankar, J. O. Marston, D. Y. Chan, S. T. Thoroddsen, *Nature* **2012**, *489*, 274.
[23] J. T. Pham, M. Paven, S. Wooh, T. Kajiya, H. J. Butt, D. Vollmer, *Nat. Commun.* **2017**, *8*, 905.
[24] G. G. Wells, R. Ledesma-Aguilar, G. McHale, K. Sefiane, *Nat. Commun.* **2015**, *6*, 6390.
[25] R. Abdelaziz, D. Disci-Zayed, M. K. Hedayati, J. H. Pohls, A. U. Zillohu, B. Erkartal, V. S. Chakravadhanula, V. Duppel, L. Kienle, M. Elbahri, *Nat. Commun.* **2013**, *4*, 2400.

[26] F. Celestini, T. Frisch, Y. Pomeau, *Soft Matter* **2013**, *9*, 9535.

[27] M. Shi, X. Ji, S. Feng, Q. Yang, T. J. Lu, F. Xu, *Sci. Rep.* **2016**, *6*, 28574.

[28] G. Dupeux, T. Baier, V. Bacot, S. Hardt, C. Clanet, D. Quéré, *Phys. Fluids* **2013**, *25*, 051704.

[29] M. Adda-Bedia, S. Kumar, F. Lechenault, S. Moulinet, M. Schillaci, D. Vella, *Langmuir* **2016**, *32*, 4179.

[30] D. Saranadhi, D. Chen, J. A. Kleingartner, S. Srinivasan, R. E. Cohen, G. H. McKinley, *Sci. Adv.* **2016**, *2*, 1600686.

[31] C. Antonini, I. Bernagozzi, S. Jung, D. Poulikakos, M. Marengo, *Phys. Rev. Lett.* **2013**, *111*, 014501.

[32] M. Shi, F. Frank, L. Wang, F. Xu, T. J. Lu, C. P. Grigoropoulos, *Phys. Fluids* **2019**, *31*, 042106.

[33] Y. S. Song, D. Adler, F. Xu, E. Kayaalp, A. Nureddin, R. M. Anchan, R. L. Maas, U. Demirci, *Proc. Natl. Acad. Sci. USA* **2010**, *107*, 4596.

[34] U. Demirci, G. Montesano, *Lab Chip* **2007**, *7*, 1428.

[35] R. E. l. Assal, S. Guven, U. A. Gurkan, I. Gozen, H. Shafiee, S. Dalbeyler, N. Abdalla, G. Thomas, W. Fuld, B. M. Illigens, *Adv. Mater.* **2014**, *26*, 5815.

[36] R. C. Hendricks, K. J. Baumeister, *Heat Transfer and Levitation of a Sphere in Leidenfrost Boiling*, National Aeronautics and Space Administration, Washington, D.C **1970**.

[37] Brookhaven National Laboratory, *Selected Cryogenic Data Notebook*, Sections I–IX, Vol. *1* (Eds: J. Jensen, R. G. Stewart, W. Tuttle, H. Brechna, A. G. Prodell), Brookhaven National Laboratory, Upton, NY **1980**.

[38] E. Baly, F. Donnan, *J. Chem. Soc., Trans.* **1902**, *81*, 907.

[39] S. K. W. Tou, C. P. Tso, *Int. Commun. Heat Mass Transfer* **1997**, *24*, 879.

[40] R. T. Jacobsen, R. B. Stewart, *J. Phys. Chem. Ref. Data* **1973**, *2*, 757.

[41] R. C. Hendricks, K. J. Baumeister, in *Advances in Cryogenic Engineering*, Vol. *16* (Eds: K. D. Timmerhaus), Springer, Boston **1971**.

[42] A. Gauthier, C. Diddens, R. Proville, D. Lohse, D. van der Meer, *Proc. Natl. Acad. Sci. USA* **2019**, *116*, 1174.

[43] M. Shi, K. Ling, K. W. Yong, Y. Li, S. Feng, X. Zhang, B. Pingguan-Murphy, T. J. Lu, F. Xu, *Sci. Rep.* **2015**, *5*, 17928.

[44] S. Jabrane, J. Letoffe, P. Claudy, *Thermochim. Acta* **1995**, *258*, 33.

[45] J. Choi, J. C. Bischof, *Cryobiology* **2010**, *60*, 52.

[46] H. Ren, Y. Wei, T. Hua, J. Zhang, *Cryobiology* **1994**, *31*, 47.

[47] P. Boutron, P. Mehl, *Cryobiology* **1990**, *27*, 359.

[48] P. Boutron, A. Kaufmann, *Cryobiology* **1979**, *16*, 557.

[49] P. Boutron, *Cryobiology* **1986**, *23*, 88.

[50] W. M. Haynes, *CRC Handbook of Chemistry and Physics*, 95th ed., CRC Press, Boca Raton, London, New York **2014**.